Eur. Phys. J. A (2016) **52**: 24
DOI 10.1140/epja/i2016-16024-3

THE EUROPEAN PHYSICAL JOURNAL A

Regular Article – Experimental Physics

Trojan Horse measurement of the ^{18}F(p, α)^{15}O astrophysical S(E)-factor

R.G. Pizzone[1,2,a], B.T. Roeder[1], M. McCleskey[1], L. Trache[1,3], R.E. Tribble[1,4], C. Spitaleri[2,5], C.A. Bertulani[6], S. Cherubini[2,4], M. Gulino[2,7], I. Indelicato[2,5], M. La Cognata[2], L. Lamia[5], G.G. Rapisarda[2,5], and R. Spartá[2,5]

[1] Cyclotron Institute, Texas A& M University, College Station, TX, USA
[2] Laboratori Nazionali del Sud - INFN, via S. Sofia 62, 95123 Catania, Italy
[3] IFIN-HH, Bucharest-Magurele, Romania
[4] Brookhaven National Laboratory, USA
[5] Dipartimento di Fisica e Astronomia, Università degli Studi di Catania, Catania, Italy
[6] Department of Physics and Astronomy, Texas A&M University-Commerce, Commerce, USA
[7] KORE University, Enna, Italy

Received: 4 November 2015 / Revised: 11 December 2015
Published online: 12 February 2016 –
Communicated by C. Broggini

Abstract. Crucial information on novae nucleosynthesis is linked to the abundance of ^{18}F, which, due to great improvements in gamma-ray astronomy, can be detected in explosive environments. Therefore, the reaction network producing and destroying this radioactive isotope has been extensively studied in the last years. Among those reactions, the ^{18}F(p, α)^{15}O cross section has been measured by means of several dedicated experiments, both using direct and indirect methods. The presence of resonances in the energy region of astrophysical interest has been reported by many authors. In the present work a report on a recent experiment performed via the Trojan Horse Method (THM) is presented and the results are given and compared with the ones known in the literature, both direct and indirect. Data arising from THM measurements are then averaged and the reaction rate calculated in the novae energy range.

1 Introduction

Gamma-ray emission from novae detected in dedicated satellite-borne experiments has become a probe for understanding novae explosions as well as the structure of such exotic stellar objects. In particular, it was noted [1] that electron-positron annihilation should occur in nova envelopes, since short-lived β^+ unstable radioactive nuclei (*i.e.*, positron emitters) are synthesized during the explosion, according to the present models. The 511 keV line might be one of the main observable features. Specifically, positrons emitted by ^{18}F may have the special feature to be emitted (and then quickly annihilated) at the moment (around 110 minutes, half-life of ^{18}F) when the novae envelope starts to be transparent to the γ-radiation [1–3].

^{18}F appears to be produced in the novae inner shells via the Hot-CNO cycle according to several authors [2]. In particular the production path goes through:

$$^{16}\mathrm{O}(\mathrm{p},\gamma)^{17}\mathrm{F}(\mathrm{p},\gamma)^{18}\mathrm{Ne}(\beta^+)^{18}\mathrm{F},$$

or

$$^{16}\mathrm{O}(\mathrm{p},\gamma)^{17}\mathrm{F}(\beta^+)^{17}\mathrm{O}(\mathrm{p},\gamma)^{18}\mathrm{F},$$

while its destruction is mainly connected with the following processes: ^{18}F(p, α)^{15}O or ^{18}F(p, γ)^{19}Ne. Thus the cross sections and the related reaction rates for all the cited reactions and in particular for the ^{18}F(p, α)^{15}O reaction should be measured in the astrophysically relevant Gamow window [4], of the order of few hundreds keV (corresponding to $0.05 \leq T_9 \leq 0.5$).

In the last decade this reaction has been widely studied and, in particular, great efforts have been devoted to its study by means of direct measurements at the relevant astrophysical energies. Such a measurement appears to be very challenging not only for the involved energy range which leads to tiny cross sections but also because the ^{18}F is a radioactive isotope, so it requires dedicated techniques to be produced.

Starting from the beginning of this century many experimental groups have tried to measure the astrophysical $S(E)$-factor for the ^{18}F(p, α)^{15}O reaction. A first direct experiment was performed by [5] focusing on the resonance at $E_{\mathrm{cm}} = 330$ keV and its strength. Other measurements were then performed in the following years by several groups with different methodologies, *e.g.*, [6–14]. Up to now many uncertainties are still present on the low-energy resonance and its width, thus affecting the determination

[a] e-mail: rgpizzone@lns.infn.it

of the reaction rate at the temperatures relevant for astrophysics and, consequently, the novae nucleosynthesis. Therefore new experimental investigation, especially focused in the novae nucleosynthesis Gamow window, are mandatory.

2 Method

Alternative and challenging ways to obtain the bare nucleus cross section, σ_b, for charged-particles at sub-Coulomb energies have been provided by indirect methods. Among them, the Trojan Horse Method (THM) [15–19] is particularly suited to investigate binary reactions induced at astrophysical energies by neutrons or charged particles by using appropriate three-body reactions. The THM allows one to avoid both Coulomb barrier suppression and electron screening effects, thus preventing the use of extrapolations. The method has proven very helpful in the last two decades for application to several aspects of nuclear astrophysics research like primordial nucleosynthesis [20, 21], the lithium problem [22, 23], AGB nucleosynthesis [24], light elements depletion in stars [25]. In all those cases it has involved the interaction of stable nuclei with p, α or n. Thus, the method can be regarded as a powerful indirect technique to get information about bare nucleus cross section for reactions of astrophysical interest, which leads to new reaction rates determination.

The basic assumptions of the Trojan Horse Method (THM) have already been reviewed recently in [19]. Here we shall just recall that this method is based on the quasi-free (QF) breakup reaction mechanism, which allows us to derive indirectly the cross section of a two-body process from the measurement of a suitable three-body one. In particular, the QF reaction mechanism specializes in the THM approach, relevant for astrophysical applications, when the incident energy is chosen so as to overcome the Coulomb barrier of the interacting nuclei. The Trojan Horse nucleus breaks up into a participant particle and a spectator one. Most used candidates as a Trojan Horse nucleus are deuteron and ^{6}Li but also ^{3}He has been successfully used [26]. The breakup process can then be thought as occurring within the nuclear region, so that Coulomb repulsion effects are greatly reduced. As a consequence, the method also becomes insensitive to problems connected with the electron screening effect. The THM has been extensively applied to reactions of astrophysical interest induced by stable beams [27–31]. The first measurement with radioactive ion beams by means of THM was discussed in [32] where the ^{18}F(p, α)^{15}O reaction was studied for the first time by means of the THM. In this paper we will apply the method to a new experimental run for the ^{18}F(d, αn)^{15}O measurement in order to obtain relevant information on the ^{18}F(p, α)^{15}O cross section at energies relevant for astrophysics (see fig. 1). This will help to confirm the indirect data already obtained in [32] and improve the statistics.

In the ^{18}F(d, αn)^{15}O process, the QF break-up is identified and selected, with deuteron splitting into its constituents p and n, whereby n is regarded as the spectator

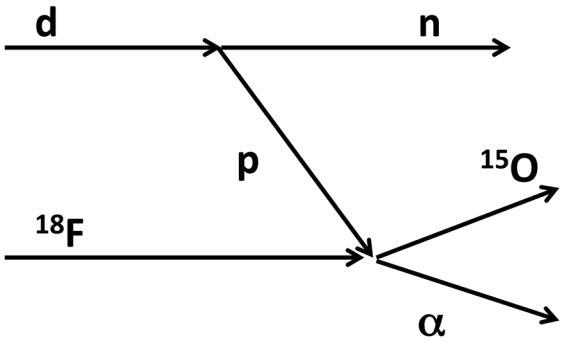

Fig. 1. Schematic representation of the quasi-free mechanism of interest in the three-body reaction used in the Trojan Horse method. The upper vertex marks the deuteron break-up while the lower vertex marks the half-off-energy shell process ^{18}F(p, α)^{15}O.

to the ^{18}F(p, α)^{15}O virtual reaction. Moreover, appropriate kinematics conditions can be selected so that the ^{18}F(p, α)^{15}O binary reaction can then take place at low interaction energies, in principle even negligible, according to the post collision prescription:

$$E_{\rm cm} = E_{\alpha-^{15}{\rm O}} - Q_{2b}, \qquad (1)$$

where $E_{\alpha-^{15}{\rm O}}$ is the relative energy between the detected α and ^{15}O while Q_{2b} (= 2.88 MeV) is the Q-value for the ^{18}F(p, α)^{15}O process.

According to the Plane Wave Impulse Approximation (PWIA), the three-body differential cross section measured in an α-^{15}O coincidence experiment can be expressed in terms of the two-body one as

$$\frac{{\rm d}^3\sigma}{{\rm d}E_{\alpha_1}{\rm d}\Omega_\alpha{\rm d}\Omega_{\rm O}} \propto (KF)|\Phi(\boldsymbol{p}_s)|^2 \left(\frac{{\rm d}\sigma}{{\rm d}\Omega}\right)^{\rm HOES}, \qquad (2)$$

where KF is a kinematical factor. The experimental spectator momentum distribution $|\Phi(\boldsymbol{p}_s)|^2$ is related to the p-n relative motion in the ^{2}H nucleus with $({\rm d}\sigma/{\rm d}\Omega)^{\rm HOES}$ the half-off-energy shell binary cross section of astrophysical interest.

Experimental evidence for a QF contribution in the ^{18}F(d, αn)^{15}O process process has been obtained in a different experimental run in a wide energy range [32].

Sequential decay processes (SD), which usually predominate in three-body reactions, have shown to be unimportant in large parts of the selected phase-space region at the present energy [32]. Since the ^{2}H momentum distribution is known (at least within a given range of the spectator momentum, see [33]), eq. (2) can be inverted to obtain the two-body cross section. For the target break-up, one expects a maximum in the QF contribution at the kinematical conditions where the spectator energy is zero, thus reflecting the neutron momentum distribution in ^{2}H, which shows a maximum at $p_s = 0$, since the relative p-n motion is mainly l = 0 [33]. This gives rise to the choice of the detection angles for the outgoing α and ^{15}O particles. They are calculated using three-body kinematics under the condition that the spectator energy, $E_{\rm n}$,

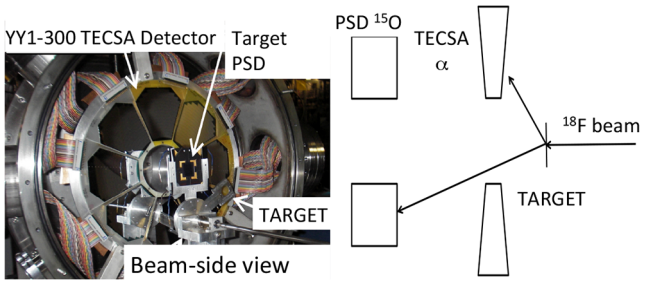

Fig. 2. Schematic view of the experimental setup used in the experiment as described in the text (right). A beam-side view of the experimental apparatus is portrayed on the left side of the picture.

is null and are referred to as the *quasi-free angles* in the standard prescriptions of the THM.

Since the Coulomb barrier is assumed to be overcome in the entrance channel, the obtained half-off-energy shell cross section, $(\mathrm{d}\sigma/\mathrm{d}\Omega)^{\mathrm{HOES}}$, should be the nuclear part only of the cross section for bare-nuclei, without the Coulomb barrier and also without electron screening effects. Moreover, the nuclear cross section is obtained within an arbitrary normalization constant to be matched to direct measurements, so that direct data have to be available at energies suitable for the normalization procedure. The agreement between the two cross sections at higher energies and the subsequent normalization represents indeed a necessary requirement for the application of the THM to a reaction of astrophysical interest and constitutes a natural step also for reactions induced by radioactive ion beams.

3 Experiment

The experiment was performed at the Cyclotron Institute of the Texas A&M University where the K500 cyclotron provided a 9 A MeV ^{18}O primary beam. The MARS spectrometer [34, 35] was then used to produce a ^{18}F beam via the p(^{18}O, ^{18}F)n reaction, after energy degrading of the primary beam by means of an Al degrader (around 30 μm thick). After isotopic selection the obtained secondary beam was tuned through MARS with a final energy of 52 MeV on a position sensitive detector at the target location of TECSA (TExas Edinburgh Catania Silicon Array) [36]. A beam spot of 3×5 mm was obtained after the beam optimization procedure was completed. The energy spread of the beam was around 2.5%. The isotopic ^{18}F purity of the beam was checked during the tuning and it was found that the beam was 94% pure and the intensity of the beam was about 3–4 $\times 10^5$ ions/s. All these features were verified during the data taking by inserting a dedicated PSD detector in the target position (clearly visible in fig. 2).

The beam impinged on an isotopically enriched deuterated polyethylene (CD_2) targets (98% purity). All the used targets were with a thickness in the range 400–800 μg/cm^2. The experimental set-up consisted of two silicon detector arrays working in coincidence. The TECSA array [36], made up of 8 YY1-300 Micron detectors (each one with 16 arch strips), was set at 190 mm from target covering angles in the range $\theta_\alpha = 15°$–$40°$. It was optimized for the α-particle detection. Closer to the beam axis a second detector system is placed, consisting of two position sensitive detectors (PSD's, type X1,16 strips each), placed symmetrically at 340 mm and covering angles from $\theta_{^{15}\mathrm{O}} = 3°$–$12°$ degrees. This one was aiming to the ^{15}O detection. The experimental set-up is sketched in fig. 2 and a summary of the geometrical features of the experimental set-up is reported in table 1. The disposition of the experimental setup was chosen to cover as much as possible of the QF angular range, known *a priori* from a Monte Carlo simulation. A plastic scintillator, put downstream at the very end of the experimental chamber, was used for monitoring and acquiring the overall beam current. Energy resolution of the cited detectors is around 0.8% while the angular one, in the present experimental set-up was about 0.7° for the PSD's and 1.1° for TECSA. The detectors were calibrated in energy by means of standard alpha sources and ^{18}F scattering off the CD_2 target. The position-sensitive detectors was also calibrated in position by means of a mask which was used during the calibration runs. The measurement of the energy and position of the two ejectiles gave the possibility to calculate all the kinematic variables regarding the third, undetected, particle as well as other variables of interest for the following data analysis (*e.g.*, Q-value, relative energy α-^{15}O, spectator momentum).

4 Data analysis

The first step in data-analysis was to identify the events related to the $^{18}\mathrm{F}(\mathrm{d},\alpha\mathrm{n})^{15}\mathrm{O}$ reaction from the other occurring in the target. This is accomplished by studying the kinematic locus related to the above reaction and the Q-value spectrum. Coincidences between each PSD and TECSA strips were examined and a typical plot of the particle energy detected in forward PSD detector *versus* the energy detected in TECSA is reported in fig. 3. A narrow angular range ($\approx \pm 2°$) is selected on both detectors and events coming from an appropriate Monte Carlo simulation, taking into account the geometrical properties of the experimental set-up as well as the features of the detectors, are reported as black dots. A good agreement shows up, thus allowing us further studies. Using a graphical cut which selects only the events overlapping with the Monte Carlo simulation, the Q-value spectrum is plotted in fig. 4, showing a peak compatible, within the experimental errors, with the theoretical Q-value of 0.66 MeV. From now on only the events with the Q-value ranging from 0 to 1.5 and inside the graphical cut in the kinematic locus were used for further data analysis. Considering the good beam purity (contaminants less than 6%) and after tagging on the coincidence together, the kinematical selection and Q-value spectrum, we can assume that the studied events are arising from the 3-body reaction of interest, *i.e.* $^{18}\mathrm{F}(\mathrm{d},\alpha\mathrm{n})^{15}\mathrm{O}$. The first step after

Table 1. Geometrical and physical details of the detector system used in the present measurement and discussed in the text.

Detector	Particle	Angular coverage	Distance from target	Energy resolution	Angular resolution
TECSA	α	15°–40°	19 cm	0.08%	0.7°
X1-PSD	^{15}O	3°–12°	34 cm	0.08%	1.1°

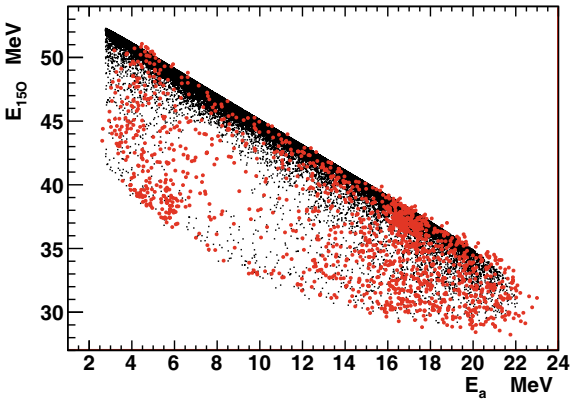

Fig. 3. Energy in the PSD (aiming for ^{15}O detection) *vs.* energy detected in TECSA (aiming for α's). Experimental events define a kinematic locus (red) that is compared with the one expected from the ^{18}F(d, αn)^{15}O reaction, as calculated in an appropriate Monte Carlo simulation (black points) for the same.

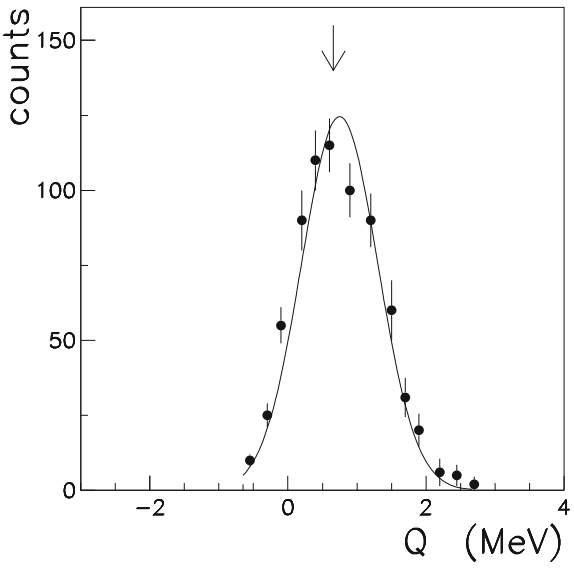

Fig. 4. Q-value spectrum for the data taken in the present experiment after selecting coincidences events in the kinematic locus defined in fig. 3. An arrow marks the expected value for the studied reaction ($Q = 0.66$ MeV).

identifying the 3-body process is to investigate the reaction mechanisms involved and to separate the quasi-free (QF) contribution from any other kind of reaction mechanism as required by the THM prescriptions. This can be done by studying, among all the available observables, the most sensitive to the reaction mechanism which is, by far, the shape of the momentum distribution, $|\varphi(\boldsymbol{p}_s)|^2$. According to the prescriptions in [37,38], the momentum distribution of the third and un-detected particle is exam-

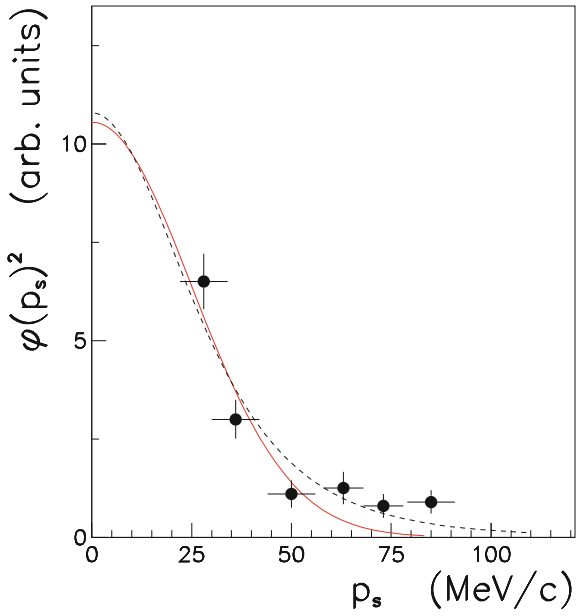

Fig. 5. Momentum distribution shape for the deuteron breakup. The comparison with a Hulthen function (dashed line) with parameters set according to [39]. The Gaussian fit to the present data is also reported (red solid line).

ined. This gives a major constraint for the presence of the QF mechanism and the possible application of the THM. In order to extract the experimental momentum distribution of the undetected particle (the spectator after the QF process is identified and selected) $|\varphi(\boldsymbol{p}_s)|^2_{\rm exp}$, the energy sharing method can be applied to each pair of coincidence detectors, selecting energy intervals, $\Delta E_{\rm cm}$. Keeping in mind the factorization of eq. (2), since $[({\rm d}\sigma/{\rm d}\Omega)_{\rm cm}]^{\rm HOES}$ is nearly constant in an adequate energy interval, one can get the shape of the momentum distribution of the undetected neutron directly from the coincidence yield divided by the kinematical factor, as calculated from a suitable Monte Carlo simulation. The obtained momentum distribution is reported in fig. 5. It is also compared with the theoretical distribution calculated from the Hulthen function (dashed line) with parameters taken from [39]. We can see how within the experimental errors the theoretical curve reproduces the experimental data, thus confirming the hypothesis that the neutron is acting as a spectator and that the process under investigation is a quasi-free mechanism. We only considered the s-wave since other contribution, *i.e.* the d-wave, were shown to be negligible [33]. According to the prescription adopted in [19] and in the standard THM approaches, only data in the $|p_s| < 55\,{\rm MeV}/c$ range were chosen and used in the further analysis.

An experimental full width at half maximum (FWHM) $\Gamma \approx 55 \pm 7\,{\rm MeV}/c$ was obtained after fitting the

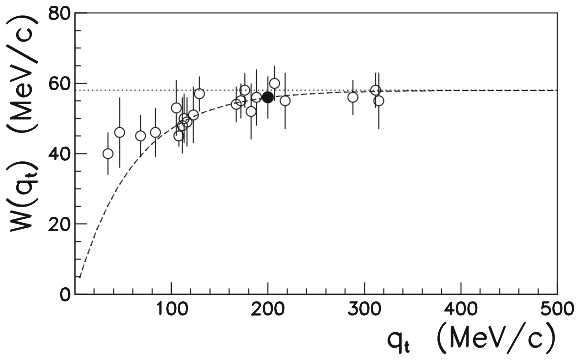

Fig. 6. Full width of the deuteron momentum distribution measured by means of the deuteron break-up as a function of the transferred momentum q_t. The full black dot marks the values obtained for the present experiment. Empty circles represent the data (table 2 of ref. [38]) and the fit (dashed line) is the same as shown in that paper. The asymptotic value is also shown as a dotted line.

experimental distribution reported in fig. 5 with a Gaussian function, and has to be compared with the asymptotic theoretical value of about 58 MeV/c. The comparison, for the present results (black circle) and data published on [38] (empty dots) as a function of the transferred momentum, q_t, is reported in fig. 6. This is coherent with results observed for other cases of deuteron break-up as well as for other isotopes. After this test we can stress the role of the neutron as a spectator to the QF process, which constitutes a solid base for the further THM application to the ^{18}F(d, αn)^{15}O reaction for retrieving information on the ^{18}F(p, α)^{15}O bare nucleus cross section at astrophysical energies.

5 Results

In the standard THM analysis, the two body cross section is derived by dividing the experimental three-body one by the product of the kinematic factor modulated by the momentum distribution of the spectator inside the Trojan Horse nucleus [19], *i.e.*

$$\left(\frac{\mathrm{d}\sigma}{\mathrm{d}\Omega}\right)^{\mathrm{HOES}} \propto \frac{\mathrm{d}^3\sigma}{\mathrm{d}E_{\alpha_1}\mathrm{d}\Omega_{\alpha_1}\mathrm{d}\Omega_{\alpha_2}} / \left(KF \cdot |\varphi_{\mathrm{exp}}(\boldsymbol{p}_s)|^2\right). \quad (3)$$

Usually the factors $KF \cdot |\varphi_{\mathrm{exp}}(\boldsymbol{p}_s)|^2$ are calculated by means of a Monte Carlo simulation, taking into account the geometrical position of the detectors. The width of the momentum distribution is set to the experimentally measured value in order to account for the distortion effects arising at low transferred momenta as discussed in [37].

The extracted $[\mathrm{d}\sigma/\mathrm{d}\Omega]^{\mathrm{HOES}}$ as a function of E_{cm}, was then compared to a previous THM run performed in CNS at the CRIB facility whose details are reported extensively in [32]. In fig. 7, the comparison between present data and those extracted in [32] are reported. We can notice a good agreement between the two THM measurements,

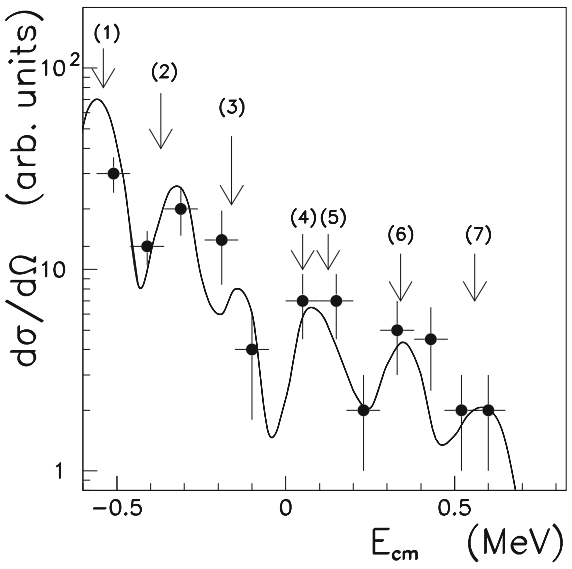

Fig. 7. Comparison of the data extracted in this experimental run (circles) with a line fitting the data from [32] (black solid line). Arrows mark the observed levels in ^{19}Ne, labeled according to table 2.

Table 2. Energy levels of ^{19}Ne in the energy range explored by the present experiment. Progressive numbers in first column correspond to energy levels in fig. 7. The ^{19}Ne* energy values are taken from [32].

Number	E_{cm} (MeV)	Energy ^{19}Ne* (keV)	$J^{(\pi)}$	Ref.
1	−0.57	5837	–	[41]
2	−0.34	6070	$3/2^+$, $5/2^-$	[10]
3	−0.16	6255	$11/2^-$	[10]
4	0.05	6460	$3/2^+$, $5/2^-$	[10,40]
5	0.13	6537	$5/2^+$, $9/2^+$	[40]
6	0.33	6755	$3/2^-$	[10,12,40]
7	0.56	6967	$5/2^+$	[40]

within the experimental uncertainties. The observed levels, marked by arrows, correspond to levels in ^{19}Ne which are reported in table 2, taken from [40] or [10]. Although the energy resolution is poorer than in the previous run (mainly due to the poorer angular resolution of the present experimental apparatus), the agreement between the two data sets confirms once again the applicability of the THM to the present reaction. The first validity check that standard THM prescriptions do recommend is to reproduce the direct excitation function. This is done by comparing the distributions measured with direct methods to the one measured by means of THM. The latter should be normalized to the direct data. The THM cross section extracted above is corrected for the penetrability factor (below the Coulomb barrier) which also makes the comparison of half-off-energy shell and on-energy shell data [19] possible. The penetrability factor is, as usual, described in terms of the regular and irregular Coulomb functions [17].

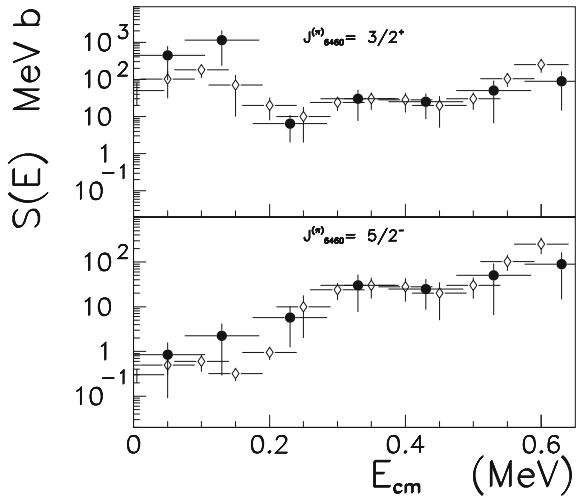

Fig. 8. Comparison of the data extracted in this experimental run (black circles) with data from Cherubini *et al.* [32] (empty diamonds). Lower panel: $S(E)$-factor extracted with the choice of $J^{(\pi)} = 5/2^-$ for the 6460 keV state in ^{19}Ne normalized to direct data from [32]. Upper panel: $S(E)$-factor for $J^{(\pi)} = 3/2^+$.

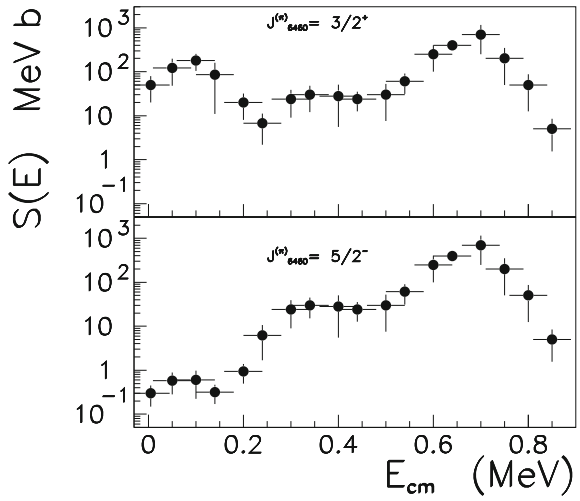

Fig. 9. Average of the present data and those from Cherubini *et al.* (2015) [32]. Lower panel: $S(E)$-factor extracted with the choice of $J^{(\pi)} = 5/2^-$ for the 6460 keV state in ^{19}Ne. Upper panel: $S(E)$-factor for $J^{(\pi)} = 3/2^+$.

THM data are also not affected by suppression effects coming from the centrifugal barrier. Assuming the J^π values of the populated ^{19}Ne excited states as in table 2, the data of each resonance have been integrated over the full angular range by means the corresponding Legendre polynomial. Finally, the data have been corrected also for the penetrability of the centrifugal barriers.

It is then possible to normalize to the direct data (after comparison with the data from [32]) at the higher possible energies (0.5–0.65 MeV) in the present case. The comparison is reported in fig. 8, where present data are represented by solid circles while the ones from [32] by diamonds. Energy states reported in table 2 were investigated in the present work; in particular the explored energy range makes relevant the contribution from the 6255 (sub threshold state), 6460, 6537, 6755, 6967 keV states of ^{19}Ne. The respective J^π were assigned accordingly as reported in table 2. A specific discussion should be done for the resonance at $E_{\rm cm} = 0.05$ MeV (corresponding to the 6460 keV state in ^{19}Ne) where two possible values of J^π were taken into account. This is clear in fig. 8. In the upper panel the black circles correspond to the choice of $J^\pi = 3/2^+$ for the 6460 keV state in ^{19}Ne following [40]. Direct data from [5,6] are reported for comparison and normalization purposes. In the lower panel the full dots represents the results for a $J^\pi = 5/2^-$ assumption for the same level as discussed in [10]. This uncertainty leads therefore to an uncertainty between the $S(E)$ lower limit (corresponding to $J^\pi = 5/2^-$ for the 6460 keV state in ^{19}Ne) and an upper limit assuming $J^\pi = 3/2^+$. Further studies (both with direct and indirect methods) and in particular the angular distribution will be necessary to improve the data quality in the low energy range. It was possible, with the present experimental run, to confirm the possibility of application of the THM to the ^{18}F(d, αn)^{15}O reaction for studying the ^{18}F(p, α)^{15}O (as reported in [32]) within the experimental errors. This was also possible in the present case where the experimental set-up and the beam production line is much simpler than the ones used in [32] (*e.g.*, simpler detection system and no beam-tracking available in the present case). This also strengthen the role of the THM which may play a leading role in the field of radioactive beams in the further years, even in cases where the experimental setup is quite simple, like the present one. However, it was possible to extract the astrophysical $S(E)$-factor by means of the THM for a reaction induced by an unstable beam, thus confirming results from [32] in all the energy range relevant for astrophysics. Further efforts are necessary to improve the energy and angular resolution of the detection system and therefore reduce the statistical error on the $S(E)$-factor. The extraction of the angular distribution will also be crucial to assign the J^π of the involved levels and will be the aim of a future, dedicated experiment, to be performed in the future with the optimized version of the detection system adopted in [32].

Data from the present experiment and the ones reported in [32] were then averaged, weighting over the respective errors. The results are reported in fig. 9 where $J^{(\pi)}$ assignment is coherent with the assumption stated above.

6 Reaction rate

The reaction rate for the ^{18}F(p, α)^{15}O reaction is calculated using the standard expression [4]:

$$R_{ij} = \frac{N_i N_j}{1+\delta_{ij}}\langle\sigma v\rangle = \frac{N_i N_j}{1+\delta_{ij}}\left(\frac{8}{\pi A}\right)^{\frac{1}{2}}\left(\frac{1}{k_B T}\right)^{\frac{3}{2}} \cdot \int_0^\infty S(E)\exp\left[-\left(\frac{E}{k_B T}+2\pi\eta(E)\right)\right]\mathrm{d}E, \quad (4)$$

where $S(E)$ is the ^{18}F(p, α)^{15}O reaction astrophysical factor and $N_{i(j)}$ is the number of nuclei of species $i(j)$.

Table 3. Reaction rate for the $^{18}F(p,\alpha)^{15}O$ as a function of temperature. The cases of $J^{(\pi)} = 3/2^+$ and $J^{(\pi)} = 1/2^-$, $3/2^-$ or $5/2^-$ are considered and reported as discussed in the text.

T_9	R_{ij} ($J^{(\pi)} = 3/2^+$) [cm^3 mol^{-1} s^{-1}]	R_{ij} ($J^{(\pi)} = 5/2^-$) [cm^3 mol^{-1} s^{-1}]
0.05	4.82×10^{-11}	9.13×10^{-9}
0.06	7.19×10^{-10}	1.51×10^{-7}
0.07	5.44×10^{-9}	1.37×10^{-6}
0.08	2.83×10^{-8}	8.01×10^{-6}
0.09	1.19×10^{-7}	3.50×10^{-5}
0.10	4.40×10^{-7}	1.20×10^{-4}
0.11	1.48×10^{-6}	3.46×10^{-4}
0.12	4.67×10^{-6}	8.61×10^{-4}
0.13	1.39×10^{-5}	1.92×10^{-3}
0.14	3.93×10^{-4}	3.88×10^{-3}
0.16	2.66×10^{-4}	1.23×10^{-2}
0.18	1.44×10^{-3}	3.43×10^{-2}
0.20	6.19×10^{-3}	7.85×10^{-2}
0.22	2.17×10^{-2}	1.65×10^{-2}
0.24	6.51×10^{-2}	3.08×10^{-1}
0.26	1.69×10^{-1}	5.58×10^{-1}
0.28	3.90×10^{-1}	9.75×10^{-1}
0.30	8.23×10^{-1}	1.65×10^{0}
0.325	1.89×10^{0}	3.09×10^{0}
0.35	3.97×10^{0}	5.61×10^{0}
0.375	7.75×10^{0}	9.90×10^{0}
0.40	1.43×10^{1}	1.76×10^{1}
0.45	4.40×10^{1}	4.79×10^{1}
0.50	1.21×10^{2}	1.26×10^{2}
0.60	6.80×10^{2}	6.88×10^{2}
0.70	2.67×10^{3}	2.68×10^{3}
0.8	7.76×10^{3}	7.77×10^{3}
0.9	1.80×10^{4}	1.80×10^{4}
1.0	3.52×10^{4}	3.52×10^{4}
1.1	6.06×10^{4}	6.06×10^{4}
1.15	7.66×10^{4}	7.66×10^{4}

We will express our reaction rates in the form $N_A\langle\sigma v\rangle$ (in units of cm^3 mol^{-1} s^{-1}), where N_A is the Avogadro number and $\langle\sigma v\rangle$ involves the integral in eq. (4) with the Maxwell distribution.

The factor $1 + \delta_{ij}$ in the denominator of eq. (4) corrects for the double counting when $i = j$. The reaction rate was evaluated for both choices of J^π discussed above thus giving rise to a lower and upper limit of its value. The calculated value corresponding to the present data is reported in table 3 and then compared with the rate extracted by [42]. Both for the case of $J^{(\pi)} = 3/2^+$ and for $J^{(\pi)} = 5/2^-$ a significant enhancement with respect to the reference data is evident; the ratio in fact ranges between 10^2 and 10^5 in the temperature window relevant for the novae nucleosynthesys ($T_9 = 0.05$–0.25). An analytic expression for the reaction rate was fitted using the

Table 4. Coefficients for the best fit of expression (5) for the reaction rate of the $^{18}F(p,\alpha)^{15}O$. The choice of different $J^{(\pi)}$ is indicated.

a_i	R_{ij} $(J^{(\pi)} = 3/2^+)$	R_{ij} $(J^{(\pi)} = 5/2^-)$
a_1	-0.357147×10^3	0.465126×10^3
a_2	0.259556	-0.229640
a_3	-0.859008×10^2	0.496752×10^2
a_4	0.569710×10^3	-0.660878×10^3
a_5	-0.153842×10^3	0.220031×10^3
a_6	0.372533×10^2	-0.631201×10^2
a_7	-0.119559×10^3	0.127164×10^3

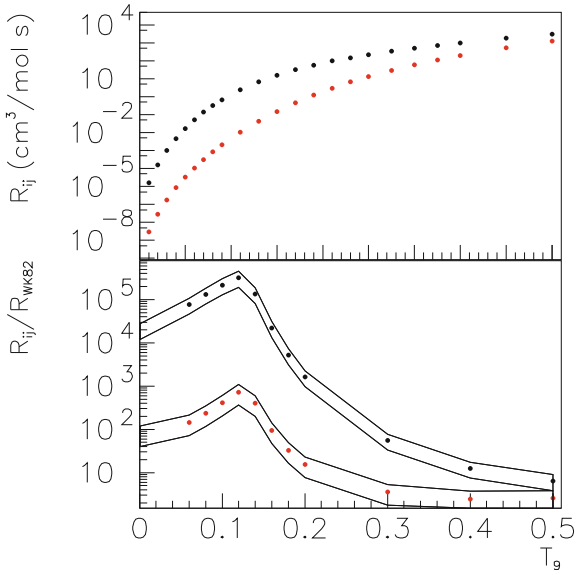

Fig. 10. Reaction rate (upper panel) as a function of T_9 calculated from the presently extracted $S(E)$ as described in the text. Red symbols mark the case of $J^{(\pi)} = 5/2^-$ while black ones the $J^{(\pi)} = 3/2^+$ one. In the lower panel it is reported its respective ratio divided by the [42] value. The error on the present calculation is represented by the solid lines.

expression

$$R_{ij} = \exp\Big(a_1 + a_2/T_9 + a_3/T_9^{1/3} + a_4 T_9^{1/3} + a_5 T_9 + a_6 T_9^{5/3} + a_7 \log(T_9)\Big) \quad (5)$$

and the resulting parameters a_i are reported in table 4.

The extracted reaction rate (see fig. 10) has significant astrophysical implications especially in the novae temperature range, where a larger rate with respect to [42] is reported. As regards the upper value $(J^{(\pi)} = 5/2^-)$ results are coherent with the reaction rate calculation from [2] while the lower limit $(J^{(\pi)} = 3/2^+)$ is much closer to the behavior of [42]. Further astrophysical applications will be investigated in a forthcoming paper.

The authors would like to thank the Cyclotron Institute accelerator division for the smooth operation of the machine. The authors also thank the mechanical workshop for the extensive work in preparation of the experiment and the INFN-LNS target laboratory and C. Marchetta for the isotopically enriched deuterated polyethylene targets and continuos assistance during the whole measurement. This work was supported by the Italian Ministry of the University under Grant No. RBFR082838 and "LNS Astrofisica Nucleare (fondi premiali)". This work was partially supported by the US-DOE grant number DE-FG02-13ER42025; the U.S. NSF Grant No. 1415656, the U.S. DOE grant No. DE-FG02-08ER41533 and the NNSA grant.

References

1. J. Jose, M. Hernanz, J. Phys. G: Nucl. Part. Phys. **34**, R431 (2007).
2. A. Coc, M. Hernanz, J. Jose, J.P. Thibaud, Astron. Astrophys. **357**, 561 (2000).
3. R. Diehl, AIP Conf. Proc. **1269**, 144 (2010).
4. C. Iliadis, *Nuclear Physics of Stars* (Wiley, 2007).
5. D.W. Bardayan, J.C. Batchelder, J.C. Blackmon, A.E. Champagne *et al.*, Phys. Rev. Lett. **89**, 262501 (2002).
6. C.E. Beer, A.M. Laird, A.St.J. Murphy, M.A. Bentley *et al.*, Phys. Rev. C **83**, 042801(R) (2011).
7. N. DeSereville, C. Angulo, A. Coc, N.L. Achouri *et al.*, Phys. Rev. C **79**, 015801 (2009).
8. J.S. Graulich, S. Cherubini, R. Coszach, S. El Hajjami *et al.*, Nucl. Phys. A **688**, 138C (2001).
9. J.S. Graulich, S. Cherubini, R. Coszach, El Hajjami *et al.*, Phys. Rev. C **63**, 011302(R) (2000).
10. A. Laird, A. Parikh, A.St.J. Murphy, K. Wimmer *et al.*, Phys. Rev. Lett. **110**, 032502 (2013).
11. Murphy *et al.*, Phys. Rev. C **79**, 058801 (2009).
12. Adekola *et al.*, Phys. Rev. C **83**, 052801 (2011).
13. Adekola *et al.*, Phys. Rev. C **84**, 054611 (2011).
14. Mountford *et al.*, Phys. Rev. C **85**, 022801(R) (2012).
15. G. Baur, C.A. Bertulani, H. Rebel, Nucl. Phys. A **458**, 188 (1986).
16. C. Spitaleri, Prob. Fund. Phys. **II**, 21 (1991).
17. C. Spitaleri, S. Typel, R.G. Pizzone, M.L. Aliotta *et al.*, Phys. Rev. C **63**, 055801 (2001).
18. C. Spitaleri, A.M. Mukhamedzhanov, L.D. Blokhintsev, M. La Cognata *et al.*, Phys. At. Nucl. **74**, 1725 (2011).
19. R.E. Tribble *et al.*, Rep. Progr. Phys. **77**, 106901 (2014).
20. R.G. Pizzone, R. Sparta, C.A. Bertulani, C. Spitaleri *et al.*, Astrophys. J. **786**, 112 (2014).
21. A. Rinollo *et al.*, Nucl. Phys. A **758**, 146c (2005).
22. R.G. Pizzone, A. Tumino, S. Degl'Innocenti, C. Spitaleri *et al.*, Astron. Astrophys. **438**, 779 (2005).
23. L. Lamia *et al.*, Astron. Astrophys. **541**, 158 (2012).
24. S. Palmerini, M.L. Sergi, M. La Cognata, L. Lamia *et al.*, Astrophys. J. **764**, 128 (2013).
25. S. Romano *et al.*, Eur. Phys. J. A **27**, 221 (2006).
26. R.G. Pizzone, C. Spitaleri, L. Lamia, C. Bertulani *et al.*, Phys. Rev. C **83**, 045801 (2011).
27. M. Lattuada, R.G. Pizzone, S. Typel, P. Figuera *et al.*, Astrophys. J. **562**, 1076 (2001).
28. C. Spitaleri, L. Lamia, S.M.R. Puglia, S. Romano *et al.*, Phys. Rev. C **90**, 035801 (2014).
29. R.G. Pizzone *et al.*, Phys. Rev. C **87**, 025805 (2013).

30. A. Tumino *et al.*, Phys. Lett. B **700**, 111 (2011).
31. A. Tumino *et al.*, Phys. Rev. C **78**, 064001 (2008).
32. S. Cherubini, M. Gulino, C. Spitaleri, M. La Cognata *et al.*, Phys. Rev. C **92**, 015805 (2015).
33. L. Lamia, M. La Cognata, C. Spitaleri, B. Irgaziev, R.G. Pizzone, Phys. Rev. C **85**, 025805 (2012).
34. R.E. Tribble, R.H. Burch, C.A. Gagliardi, Nucl. Instrum. Methods A **285**, 441 (1989).
35. R.E. Tribble, C.A. Gagliardi, W. Liu, Nucl. Instrum. Methods B **56/57**, 956 (1991).
36. B.T. Roeder, M. McCleskey, L. Trache, A.A. Alharbi *et al.*, Nucl. Instrum. Methods A **634**, 71 (2011).
37. R.G. Pizzone, C. Spitaleri, S. Cherubini, M. La Cognata *et al.*, Phys. Rev. C **71**, 058801 (2005).
38. R.G. Pizzone, C. Spitaleri, A.M. Mukhamedzhanov, L.D. Blokhintsev *et al.*, Phys. Rev. C **80**, 025807 (2009).
39. M. Zadro, D. Miljanic, C. Spitaleri, G. Calvi *et al.*, Phys. Rev. C **40**, 181 (1989).
40. C.D. Nesaraja, N. Shu, D.W. Bardayan, J.C. Blackmon *et al.*, Phys. Rev. C **75**, 055809 (2007).
41. D.R. Tilley, H.R. Weller, C.M. Cheves, R.M. Chasteler, Nucl. Phys. A **595**, 1 (1995).
42. M. Wiescher, K. Kettner, Astrophys. J. **263**, 891 (1982).